

Research on evolution process of full-layer incision of skin tissue under different laser incidences

Kehong Wang¹, Yuxin Chen¹, Jun Huang¹, Yunfeng Rui², and Wentao Fan³

¹Nanjing University of Science and Technology School of Science

²Southeast University Zhongda Hospital Department of Orthopedics

³Nanjing Medical University The Fourth School of Clinical Medicine

July 25, 2023

Abstract

Considering difficulties of achieving vertical incidence of beam in different positions of skin, it's significant to study potential effects of incidence angles of laser on incisions. Surgical platform with a 1064nm continuous fiber laser was established. Incident angle was adopted and real-time temperature fluctuations in laser operating area could be monitored. The rats were treated with laser at day 0 and day 3 after incision modeling, and H&E, Masson, Sirius Red and Immuno-histochemical staining and enzyme-linked immunosorbent assay were adopted at day 3,7,14 to analyze the performance of healing. Laser with energy density of 67.54J/mm² can effectively accelerate wound healing in vivo, in which laser with incident angle around 60° can effectively avoid scar hyperplasia. Therefore, the use of low energy laser with small deflection angle has a good clinical application prospect in promoting wound healing.

Research on evolution process of full-layer incision of skin tissue under different laser incidences

Yuxin Chen^{a*}, Jun Huang^{a*}, Kehong Wang^{a*}, Xiaopeng Li^a, Yunfeng Rui^b, Wentao Fan^c,

^a School of Material Science and Technology, Nanjing University of Science and Technology, Nanjing, China

^b Department of Orthopaedics, Southeast University, Zhongda Hospital, Nanjing, China

^c First school of clinical medicine, Nanjing Medical University, Nanjing, China

*Corresponding author: Kehong Wang, E-mail:wkh1602@126.com, Jun Huang, E-mail:huangjun@njjust.edu.cn, Yuxin Chen, Email: chenyuxin1602@njjust.edu.cn

Abstract :Considering difficulties of achieving vertical incidence of beam in different positions of skin, it's significant to study potential effects of incidence angles of laser on incisions. Surgical platform with a 1064nm continuous fiber laser was established. Incident angle was adopted and real-time temperature fluctuations in laser operating area could be monitored. The rats were treated with laser at day 0 and day 3 after incision modeling, and H&E, Masson, Sirius Red and Immuno-histochemical staining and enzyme-linked immunosorbent assay were adopted at day 3,7,14 to analyze the performance of healing. Laser with energy density of 67.54J/mm² can effectively accelerate wound healing in vivo, in which laser with incident angle around 60° can effectively avoid scar hyperplasia. Therefore, the use of low energy laser with small deflection angle has a good clinical application prospect in promoting wound healing.

Key words: Laser tissue welding; Wound healing; Incident angles; Laser automated surgical platform; Collagen remodeling

Introduction

The skin is the largest organ of the human body, playing a role in maintaining the fluids and electrolytes homeostasis, resisting physical and chemical damage, as well as preventing microbial infections^[1]. Regrettably, full-thickness skin defects are prone to occur under various injury factors, such as large-scale burns, traumatic injuries, diabetic ulcers, and vascular lesions, which seriously harmed not only the life quality of patients, but also the medical economy. Current therapeutic interventions remain far from ideal repair^[2].

Medical laser is known as an epoch-making progress in traditional surgery, and has become a special and effective means of diagnosis and treatment in many medical fields^[3-4]. In recent years, laser has made great progress in the field of biomedicine, especially in minimally invasive surgery, due to its excellent monochromatic properties, collimation and flexible energy density^[5-6]. The thermal effect produced by laser acting on biological tissue with different wavelength and energy is also different, so different types of tissue normally need different kinds of lasers^[7,23-25]. The surgical application and safety procedures of lasers are related to the degree of thermal damage^[8-9]. The degree of thermal damage is not only a function of laser parameters, such as power density, duration, pulse width, etc., but also depends on the absorption and scattering properties of tissues and thermophysical parameters such as thermal conductivity and thermal diffusivity of tissues^[10-11]. Once the heat source is determined, the tissue temperature distribution changes can be calculated according to the heat transport equations and various assumed conduction and convection boundary conditions^[12-13]. An increase in temperature can lead to cell inactivation, protein denaturation, and even vaporization and cutting of tissues^[14]. Medical laser technology, a non-contact skin tissue suture has the advantage of high immediate tensile strength^[15], fast recovery, low infection and less scar tissue and so on which has outstanding application potential in surgery, obstetrics and gynecology and cosmetic surgery^[16]. However, in practical applications, the location of the full-layer incision in the skin tissue is relatively flexible, which cannot guarantee that the laser can be vertically incident. Therefore, it is of great significance to study the evolution rule of microstructure, collagen degeneration^[17] process and content changes of important cytokines in the process of bonding full-layer incision of skin tissue by different laser incidences in order to accelerate the prognostic process for achieving the clinical progress of laser induced full-layer incision connection technology^[18-19]. Since the thickness of skin tissue is small and the photo-thermal effect between laser and skin tissue is sensitive^[20], the evolution process of microstructure corresponding to different layers of skin is an important reference to judge the healing situation of samples. Similarly, the change of macro morphology is inevitably based on the change of microstructure morphology. In this study, continuous low-power laser was performed on the back of living SD rats by different laser incident angles. The macro-morphology, microstructure morphology, fibroblast morphology, endothelial growth factor content, and the distribution of type I and III collagen were continuously characterized at fixed periods. The laser bonding processes of skin tissue was further investigated from the microscopic mechanism of healing, also the potential of laser bonding incisions in different positions have been verified theoretically and experimentally.

Materials and Methods

On the basis of great researches before, we constructed a comprehensive welding system which could meet all basic demands during the laser welding processes, as shown in Fig.1. The skin tissue connection machine used in this study consists of three parts: a laser working system, a thermograph, and an overall control system. The laser working system consists of 1064nm Nd:YAG consecutive fiber lasers, a workbench and relevant clamping devices. The thermograph consists of a Fortic near-infrared thermal imager and a control subsystem. The overall control system consists of the temperature output data processing subsystems of a laser control system and a thermal imager. The overall control system in Fig.2.1 can adjust and set the laser parameters in real time and monitor the temperature changes of skin tissues, and can regulate tissue injuries and the macroscopic condition of welding. In order to guarantee the accuracy and scientificity of experimental data, we also carry out the experiments in an ultra-clean laser surgery area, as shown in Fig.1.

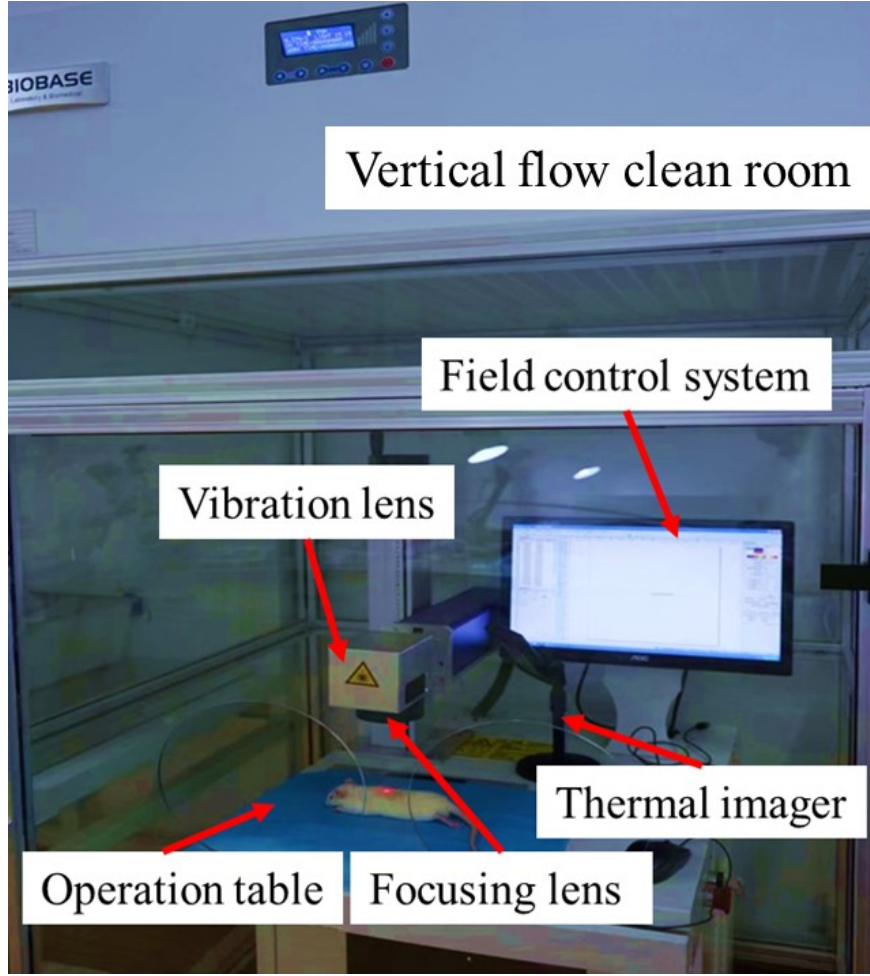


Fig.1 Ultra-clean Low energy Nd:YAG 1064nm laser automated surgical platform

On the basis of previous experiments, we have summarized the optimized basic laser parameters including laser power, laser scanning path, defocus amount, wavelength and scanning speed^[27-28]. Through comprehensive analysis on both macroscopic and microscopic of skin tissue after laser welding, combined with the body temperature and thickness of rats, we further optimized the laser parameters as shown in table.1. And we operated on the wounds of the rats on day 0 and day 3 of the healing cycle.

Table.1 Experimental parameters

No.	Defocus amount	Power/w	Speed/mm. s ⁻¹	Scanning mode ^[26]	Energy density/J.mm ⁻²	Incident angle/°
1	-1	7	100	Simulated Stich	67.543	90
2						60
3						30

Before we designed our experimental parameters, we tried to start the incident angles from a very small degree which far below 30°, however, we found that when incident angle is below 30°, the incident angle of laser is too small to focus on the plane of the wound, and the laser beam could not transfer the heat and photon into full layer of tissue. When incident angle was below 30°, only the epidermis and upper dermis can

receive laser energy which on the other hand led to severe heat damage of wound surface. So, we started our experiments using incident angles larger than 30° . We designed three different incident angles which vary from 30° to 90° in order to simulate different position of potential wound on the back of rats, the scheme diagram is shown in Fig.4(C). Because of the symmetry of the laser incidence, we performed a deflected incidence of the rat wound on the fixed side.

All SD rats were purchased from Changzhou Covens Laboratory Animal co., LTD and familiarized with their new environment for a week. All rats (180-220g) used were male and fed under SPF (specific pathogen-free animal) facility with a 12:12h light–dark cycle. All surgical procedures were conducted under animal care protocols approved by the Ethics Committee of Nanjing University of Science and Technology.

45 rats were randomly assigned to each experimental group and distributed by three test indexes with four time points. Fifty rats were randomly divided into three different groups [90° ($n = 5$), 60° ($n = 5$), and 30° ($n = 5$)] at each time point: 3, 7, 14 and 24 days, and each group had one control rat.

After anaesthetization (1.5–3 vol.% Isoflurane), the dorsal surface hairs were shaved and then incised with a 15mm sterile bistoury, all the operation was carried out in Ultra-clean platform as shown in Fig.2(A). The incision area could be observed in Fig.2 which could also be regarded as welding area in the follow-up laser processing. The length of full-thickness wound is 3cm and the depth of wound is 2mm. The whole processes of animal modeling and laser bonding were conducted in specialized ultra-clean workshop as shown in Fig.2(A) and (B). Incision wound sites after laser treatments were covered with air-permeable Tegaderm (3 M, St. Paul, MN) tape as seen in Fig.2(C). Throughout the experiment, rats were housed individually post-operation with access to food and water ad libitum, kept under controlled conditions of humidity (50%–70%), temperature (20–22), light: dark cycle (12 h:12 h), and free access to food and water. The digital photographs were used to monitor the wound closure over time on days 0, 3, 7, 14 and 21 post surgery. The wound healing progress was analyzed using *Image J* software and calculated based on the wound reduction area using the following equation Then, the wound area was determined by tracing the wound margins with *Image J* software and an image analysis program (Adobe Photoshop cs6). The degree of wound healing is expressed as a percentage of original wound size. Rats were sacrificed and their dorsal skin was surgically removed for histological analysis^[29-33].

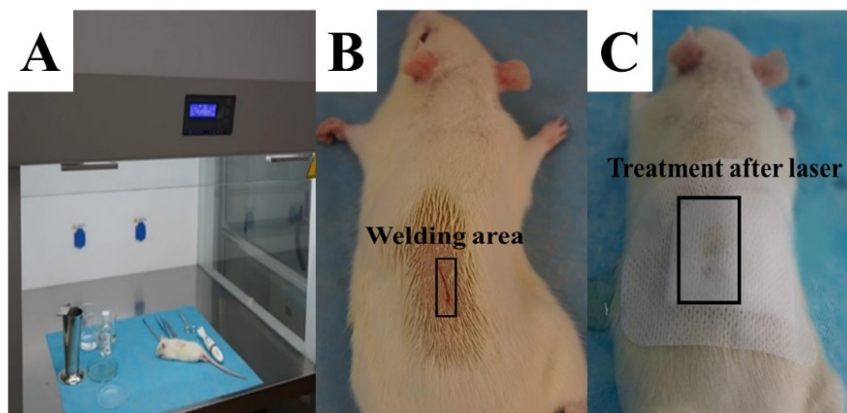


Fig.2 Representative images of surgical preparation. (A) Ultra-clean surgical preparation area. (B) After the animal model operation (C) Treatment after laser welding.

The wound healing progress was analysed using ImageJ software and calculated based on the wound reduction area using the following equation(1):

$$Healing\ Percentage(\%) = \left(\frac{WA_0 - WA_t}{WA_0} \right) \times 100\% \quad (1)$$

where WA_0 is the wound area at the wounding day (day 0) and WA_t is the wound area at each respective day.

Results

Macroscopic healing performances in vivo

Figure 3 depicts the laser welding model used in our animal experiment. The procedure begins with making a full-thickness incision on the rats' back. Following this, we created a solution by combining 5% Bovine Serum Albumin (BSA) and 10% normal saline solution which was then applied to the wound every 30 seconds throughout the laser operation. We adopted a Zigzag pattern (as represented in Fig.4(B)) to mimic the Suture technique commonly used in surgical operations. As seen in Fig.3(C), we administered two rounds of laser treatment during the healing process, with the initial procedure on day 0 and the subsequent one on day 3, each session lasting for 3 minutes. We monitored the wound recovery at intervals: 3-, 7-, 14-, and 24-days post-treatment. Although the healing stages were generally completed by the 14th day, we continued observations until day 24 to comprehensively document and analyze all aspects of the healing and prognostic cycles. To probe the laser's potential in accelerating wound healing in rats and to examine the impacts of varying laser incident angles, we established four groups: control (no treatment), and groups exposed to lasers angled at 90°, 60°, and 30° respectively.

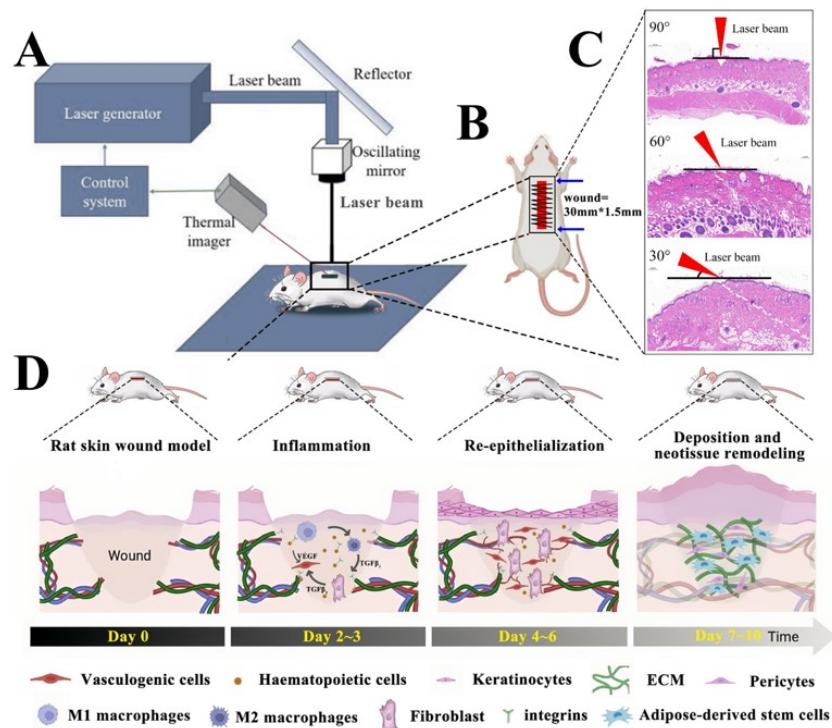


Fig.3 Model of laser treatment in wound of rats. (A) laser automated surgical platform with different incident angles. B) Schematic cross-sectional view of the treatment process of rat skin tissue. C) Schematic of laser scanning path-Zigzag .

We monitored and quantitatively measured the wound healing process at pre-determined intervals post-operation as depicted in Fig.4(A). The observations revealed innate self-healing capabilities in rats as evidenced by the continuous reduction in wound area in the control group, despite wounds remaining unhealed after 24 days without any additional treatment. It appears that low-energy laser treatment at 1064nm can

foster wound healing to an extent, as all three laser-treated groups exhibited smaller wound areas compared to the control group at every time-point post-treatment. Notably, complete recovery was achieved in all laser-treated groups within 14 days, marking a healing period 41.7% shorter than that of the control samples. As per Fig.4(C) and Fig.4(B), the 30°Laser samples showed the quickest healing speed during the first stage (initial 3 days) of laser welding, while the 90°Laser samples exhibited the fastest healing speed in the second stage. For the 60°Laser samples, even though the initial healing speed wasn't particularly prominent, the healing processes post the second laser weld were the most significant. It remains challenging to determine the optimal parameter group based solely on the trend of healing speed and wound size since factors like collagen fiber disposition, distribution of inflammatory factors, and varying types of collagen content are all vital indicators of healing performance. To further scrutinize the differences between incident angles and the mechanism of laser welding tissue, we proceeded with comprehensive characterization and analysis of cells, collagen, and functional protein groups during the healing process. This data has been incorporated into Fig.4(C) and will be detailed in the following sections.

Fig.4 Whole process of wound healing. (A) Representative images of macro appearances of rats during whole healing processes in three groups. (B) Schematic diagram of the wounds managed by different laser treatments in 24 days. (C) Quantitative data of wound sizes at different time points ($n \frac{1}{4} 3$). (D) Quantitative data of wound healing ratio at different time points ($n \frac{1}{4} 3$). Data represent mean \pm SD; *, $P < 0.05$, **, $P < 0.01$.

Microstructures of rats after laser welding with different incident angles

In trauma treatment, the wound healing process is typically segmented into stages: the inflammatory response stage, the granulation stage, and the epithelial formation stage. These stages often overlap with each other. Figure 5 presents Hematoxylin and Eosin (H&E) stained images of the wound tissue at specific time points, which include days 3, 7, and 14. The figure distinctly reveals noticeable differences in the microstructure of samples throughout the healing process under varied laser incident angles.

On day 3, post the first laser welding, the incision location and gap are still clearly visible at 200 μm magnification. Following the first laser weld, the most pronounced recovery was observed in the 90° laser and 30° laser groups; the wound incision gap in the dermis layer was considerably reduced, and partial remodeling of the collagen in the dermis had occurred through integrin interactions. On the contrary, the samples in the 60° group exhibited significant epidermal gaps and it remained challenging to discern clear collagen deposition in the dermis.

Following the second laser welding on day 3, marked improvements were noted across all groups, with particularly tremendous healing progress in both the 90° and 30° laser groups. At this stage, the incision's micromorphology was barely noticeable in all three groups, and re-epithelialization of all samples had commenced along with new granulation formation. This re-epithelialization process is pivotal to accelerating dermal healing; the beneficial thickening of the upper epidermis serves as a bio-functional barrier established early in the wound healing process. This barrier plays a crucial role in preventing excessive transdermal water loss and further wound infection.

By the 14th day of the healing process, it was observed that any existing gaps in the wound incision had entirely disappeared. The upper epidermis was completely covered, and a dense new collagen network structure was evident in the dermis.

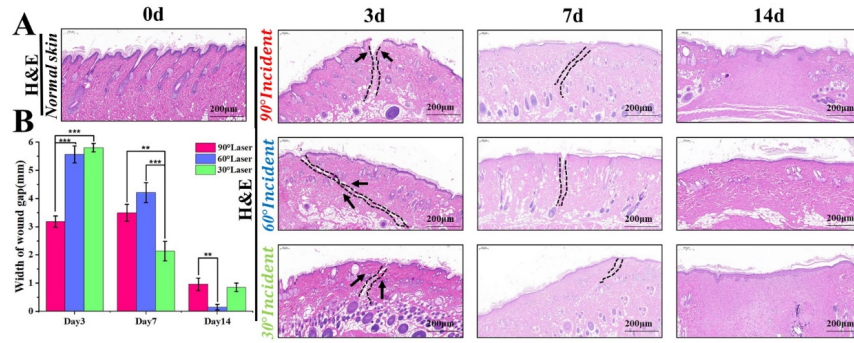


Fig.5 Pathological examination of wound tissue (A) Representative images of evolution of microstructure during healing processes by H&E staining ($\times 400$). (B) Quantitative data of width of wound gap after the two stages of laser welding at different time points ($n = 3$). Data represent mean \pm SD; *, $P < 0.05$, **, $P < 0.01$.

Overall collagen proliferation during wound healing

In Masson's Trichrome staining, collagen fiber is represented by blue coloration, as depicted in Fig.6. On the third day after the first laser welding, it was observed that collagen deposition in the 90deg laser group concentrated mainly in the dermis, becoming more pronounced near the subcutaneous fat layer. Alterations in the structure of some subcutaneous fat were visible, including finer, smaller fat particles and larger fibroblast nuclei. In contrast, the 60deg laser group displayed significant collagen deposition distributed within the dermis and epidermis surrounding the wound, with this group demonstrating the most substantial deposition area according to the intensity of the blue shades in Fig.6.

By day 7, there was a noticeable difference from the initial stage of laser welding. The collagen distribution in all three laser groups was finer and more even compared to day 3, signifying that most deposited collagen underwent further remodeling to form a dense network post the second laser welding—an indicative feature of extraordinary healing performances. However, incision marks were still visible in the cross-section provided by Fig.6, indicating that the wound was yet to fully heal and remained in the fibroblast proliferation phase. In conclusion, the densest collagen network was found in the 90deg laser group, followed by the 60deg and 30deg laser groups respectively.

14 days into the healing process, notable changes were observed. Firstly, collagen in both the 90deg and 30deg laser groups had further proliferated, and fibroblast levels essentially returned to normal. The 90deg laser group showed only slight gaps in collagen, and the dermis area affected by the laser exhibited complete newly formed fine collagen tissue. In contrast, the samples in the 60deg laser group demonstrated restoration closer to the original collagen texture, closely resembling the dermis collagen of normal skin. This suggests that the samples in the 90deg and 30deg laser groups may require an extended healing cycle due to their overly fine collagen network and fibroblast levels lower than the pre-treatment state. These conditions could result in decreased elasticity of the collagen network and potential abnormal proliferation post-collagen cracking [43-45]. Such phenomena might be caused by the concentrated energy of the 90deg laser, which, besides promoting fibroblast proliferation, also inflicts additional thermal damage, causing the destruction and potential loss of biological activity in some hematopoietic cells and integrins. Although the healing process was significantly enhanced, it remained challenging to ensure the thickening and hardening of the collagen scaffold post the epithelial regeneration stage.

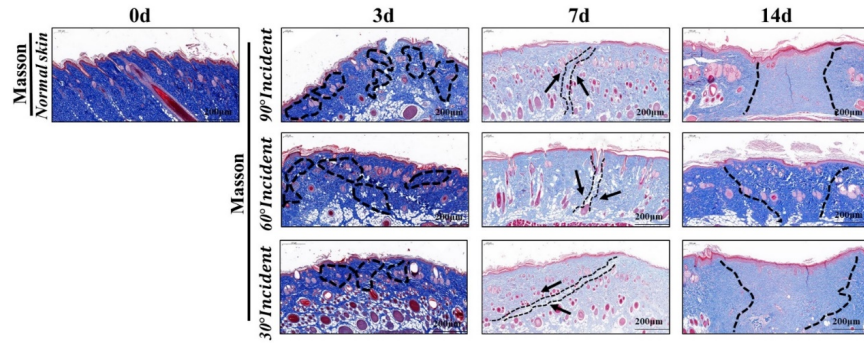


Fig.6 Pathological examination of wound tissue — Masson's Trichrome staining of Tissue

Type I and Type III proteins have their main distribution in the dermis, while Type IV and Type VII are chiefly located within the subcutaneous tissue [47-50]. Before delving into a specific analysis of the collagen types and their distribution in samples at various time points as represented in Fig. 7, an elementary examination was conducted on the Sirius Red-stained microstructure under a 400x magnification. Initially, on the third day subsequent to the initial laser welding, sporadic deposition of COL-1 fibers around the wound was observed, with the most considerable being in the 90° laser group. After the application of the second laser welding, the groups subjected to deflected laser incident angles presented a significantly greater COL-I fiber deposition compared to the 90° laser group. This observation suggests that following two instances of laser welding, the wound area in the 90° laser group had become more supple and softer. COL-1 fibers, which are densely aligned and relatively rigid, offer structural support, whereas COL-3 fibers contribute to the flexibility of the tissue, primarily affecting the skin's softness. In normal tissues, the Type I to Type III collagen ratio typically fluctuates between 1:1 and 2:1. Any significant deviation from this range may suggest instability in the skin's collagen structure [51-52].

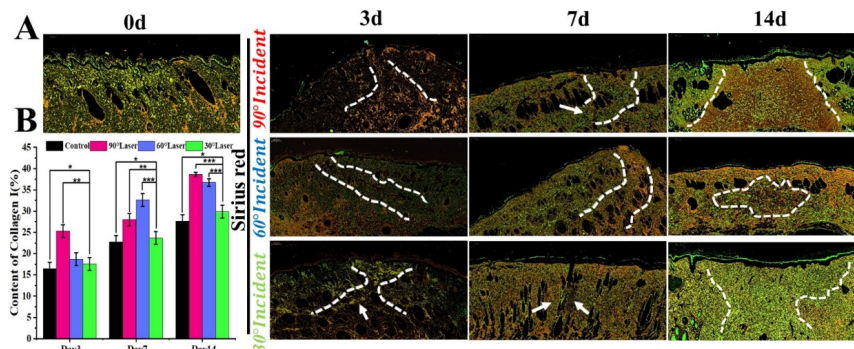


Fig.7 Pathological examination of wound tissue (A) Representative images of evolution of microstructure during healing processes by Sirius Red staining (x400). (B) Quantitative data of Content of COL-1 fiber after the two stages of laser welding at different time points (n = 3). Data represent mean ± SD; *, P < 0.05, **, P < 0.01.

Overall cell proliferation during wound healing in rats

Immunofluorescence staining was utilized to perform immune expression of Fibronectin antibodies. As depicted in Fig.8(A), it showcases the progressive evolutions in fibroblast expression throughout the entire healing process—from day 3 up until day 14—following two laser welding sessions. On the third day after the initial laser welding, it was noted that fibroblast proliferation was most prominent in the 60deg laser group,

reaching a fluorescence intensity of 1.28 (as demonstrated in Fig.8(B)) after normalization, with substantial proliferation observed within the dermis. Post the second laser welding, the fluorescence expressions within the groups stabilized around a value of 1.25, and noteworthy fibroblast clustering was detected in the 60deg laser group. By day 14, the fibroblast content within the laser groups returned to normal levels, with the primary fluorescence expression concentrated within the middle and lower regions of the dermis [53-58]. The fibroblast expression in the 30deg laser group was still densely concentrated, indicating a slower healing process compared to the other two groups.

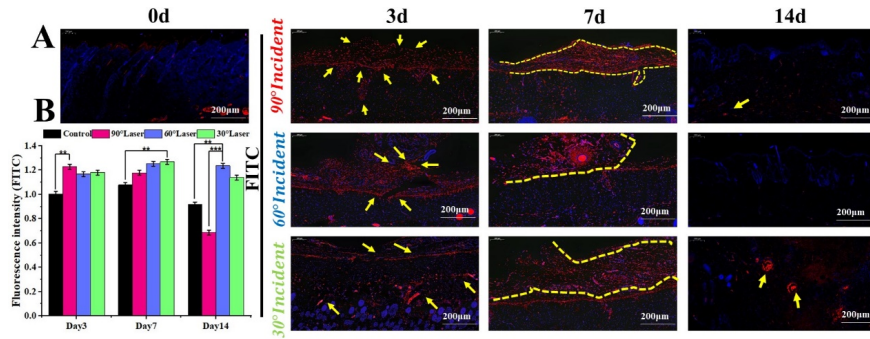
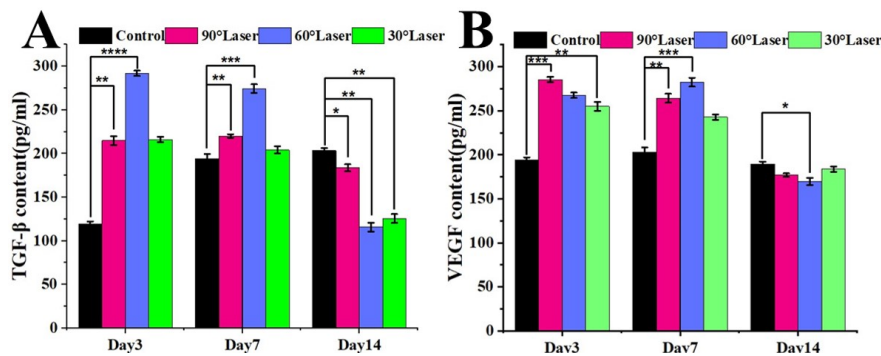


Fig.8 Representative images of wound tissue sections stained by FITC in different treatment groups on different days (Scale bar $\frac{1}{4}$ 100 μ m). (B) Quantification of the Fluorescence intensity of FITC staining in different treatment groups on different days. (n $\frac{1}{4}$ 3). Data represent mean \pm SD; *, P \leq 0.05, **, P \leq 0.01, ***, P \leq 0.001.

Throughout the healing process, Transforming Growth Factor- β (TGF- β) serves as a key regulator closely associated with overall cell proliferation. As depicted in Fig.9(A), following the initial laser welding, TGF- β secretion peaked in the 60° laser group, approximating 300 pg/ml. This suggests that a low-energy laser at a 60° incident angle could effectively activate the inflammatory response stage, stimulate M2 macrophage activity, and trigger an ample secretion of TGF- β 2 factor, thereby catalyzing fibroblast proliferation. Although the healing process in the 60° laser group showed no significant improvements after the first laser treatment, it established a solid foundation for collagen skeleton regeneration in subsequent stages. The TGF content in the 90° laser group was almost equivalent to that in the 30° laser group (\sim 200pg/ml). Following the second laser welding, the TGF levels across all groups displayed similar rankings, albeit decreased, indicating the onset of the re-epithelialization stage of healing. By day 14, the TGF level within the control group began to rise gradually, while the remaining three groups nearly returned to their normal levels. However, the TGF level in the 90° laser group remained at around 200pg/ml, suggesting a potential recurrence of scarring.



As demonstrated in Fig.9(B), the Vascular Endothelial Growth Factor (VEGF) levels at the wound site for all

groups were quantified using ELISA methods. The data reveals that in comparison to the control group, the VEGF content experienced a significant increase following the first laser welding. Most notably, the VEGF level in the 90° laser group peaked at an impressive 276pg/ml on the third day, indicating that the laser at a 90° incidence had the most profound effect after a single laser welding session, stimulating an abundant production of VEGF. Such an observation also implied that this group had the most rapid healing process. Conversely, the 60° and 30° laser groups exhibited inferior VEGF levels, as shown in Fig.9(A). Following the second laser welding session, the 60° laser group demonstrated the highest VEGF level, whereas the VEGF content decreased in the 90° laser group. This pattern suggests that high-energy concentration at a vertical incident angle might inflict additional thermal damage to the wound tissues, whereas a 60° laser effectively promotes continued VEGF secretion by vasculogenic cells. By day 14, all laser groups registered lower VEGF levels compared to the control group. This trend indicates that while the wound had fully closed, collagen growth and metabolism within the dermis persisted beyond this point. Of note, the VEGF level in the control group was seen to be approximately 200pg/ml on the 14th day—higher than any other group—suggesting that the samples from the control group might need at least 14 additional days for complete wound closure compared to the laser groups. Throughout the entire process, the 30° laser group exhibited minimal fluctuations in VEGF levels and consequently displayed the lowest healing efficiency among the laser groups. Despite the lack of pronounced changes in the VEGF content of the 30° laser group, it consistently maintained significantly higher levels than the control group, demonstrating the capacity of low-energy 1064nm lasers to effectively expedite wound healing.

Fig.9 Cell proliferation and differentiation of wound tissue. (A) Quantitative analysis of TGF- β content in wound tissue by the ELISA method. (B) Quantitative analysis of VEGF content in wound tissue by the ELISA method. Data represent mean \pm SD; *, P \leq 0.05, **, P \leq 0.01, ***, P \leq 0.001.

Discussions

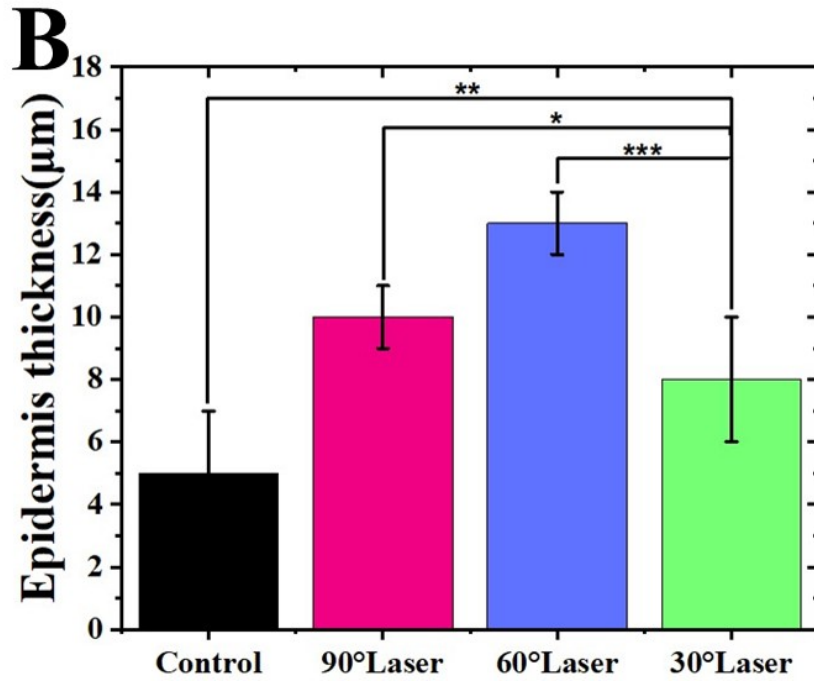
Wound healing study in vivo

Regarding the 60° laser samples, although initial healing progress wasn't particularly noticeable, the most significant healing responses were observed following the second laser welding process. However, it is challenging to categorically conclude on the optimal parameter group based solely on the trends in healing speed and wound size, as factors such as collagen fiber disposition, inflammatory factor distribution, and the concentration of different collagen types all play crucial roles in characterizing healing performance. To meticulously analyze the differences between incident angles and decipher the mechanism behind laser-welded tissue healing, we subsequently performed comprehensive characterization and analysis of cells, collagen, and protein functional groups throughout the healing process. These findings have been encapsulated in Fig.4(C), with further details provided in the subsequent sections.

Histology of wound healing site in rats

To provide a more quantitative assessment of the wound healing process at different time points, we evaluated the regenerated epithelium by measuring the length of neo-epithelial tongue and the area of neo-epithelium, as depicted in Fig.10(A). Firstly, we marked the position and length of the epithelial tongues in various groups on the third day post-healing. Following two laser welding treatments, all samples—with the exception of the control group—exhibited some degree of re-epithelialization. This indicated progression to the third stage of healing, characterized by vigorous proliferation of fibroblasts and angiogenic cells. Partial formation of collagen skeletons in the tissue's dermis was also observed, interconnected via integrin. Concurrently, keratinocytes and adipose-derived stem cells gradually increased in number while the inflammatory response subsided. Examination of Fig.10(A) revealed an abnormal upper epidermis shape in the control group, resembling a gully. Data from Fig.10(B) and (C) confirmed that the length and area of the upper epidermis in this group were the smallest among all test groups. In comparison, laser-welded samples displayed more regular epidermal regeneration. Specifically, specimens from the 90° laser group had the longest upper epidermis and largest surface area, approaching approximately 45 mm². However, it is worth noting that the wound gap distribution pattern depicted in Fig.10(B) contradicts the upper epidermis growth pattern for the 60°

and 30° laser samples. This discrepancy suggests that wound gap reduction primarily indicates the status of dermal collagen healing, whereas the regeneration process of the upper epidermis may not necessarily occur synchronously with collagen remodeling.



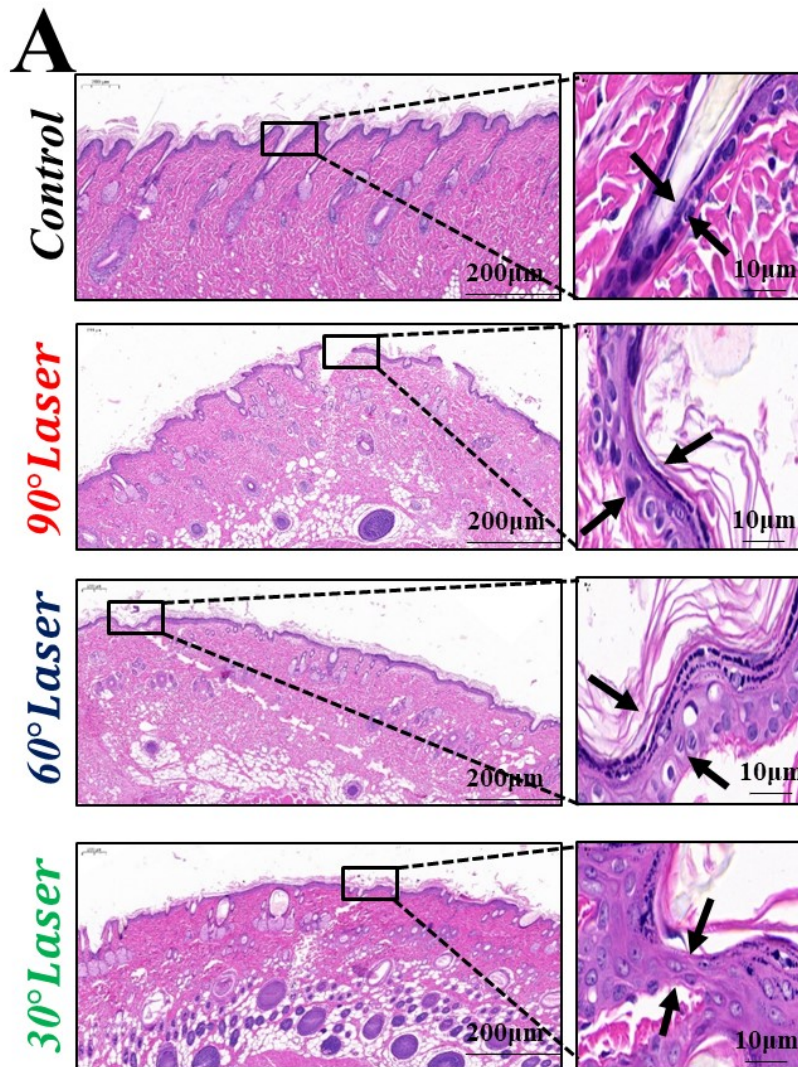


Fig.10 Representative images of upper epidermis around wound tissue sections in different treatment groups stained by H&E on day 3 (Scale bar $\frac{1}{4}$ 1 mm). (B) Quantification of the length of neo-epithelial tongue in different treatment groups on day 7 (n $\frac{1}{4}$ 3). (C) Quantification of the area of neo-epithelium in different treatment groups on day7 (n $\frac{1}{4}$ 3). Data represent mean \pm SD; *, P \leq 0.05, **, P \leq 0.01, ***, P \leq 0.001.

Following second laser welding, we proceeded with the extraction of samples on the seventh day as shown in Fig.11. Our aim was to investigate the relationship between healing efficacy and the thickness of the upper epidermis. The regeneration site of the upper epidermis was clearly marked, subsequently expanded to a 10µm scale, and the thickness of the upper epidermis was calculated. Our findings revealed that seven days post-wounding, the least degree of upper epidermal thickness was observed in the control group. Conversely, the most significant thickness was noted in the 60° laser group, followed by the 90° and 30° laser groups respectively. A prior analysis concluded that the upper epidermis exhibited optimal regenerative capacity after the initial phase of 90° laser treatment. Additionally, on the seventh day following the second round of laser welding, the thickness of the upper epidermis reached its zenith within the 60° laser group. This suggests

that the first round of laser welding at a 90° incident angle effectively triggers an inflammatory response, thus hastening the healing process [47-49]. However, the secondary laser welding at a 90° incident angle results in relatively higher thermal damage, which paradoxically hinders epithelial regeneration. In contrast, although the laser with a 60° incident angle didn't yield the most noticeable effect after the first stage of laser welding, it did ensure reasonable thermal damage based on the initial laser welding. Consequently, the healing process was expedited following the second laser procedure.

Regarding laser welding at 30° incident angle, less epithelial regeneration was observed in comparison to the other groups (as shown in Fig.10(A) and Fig.11(A)). This implies that the healing process was more convoluted and slower for these samples. More specifically, epithelial hyperplasia was accompanied by inflammation, and there was a failure to achieve 100% heat transfer in the wound area at the level of the dermis.

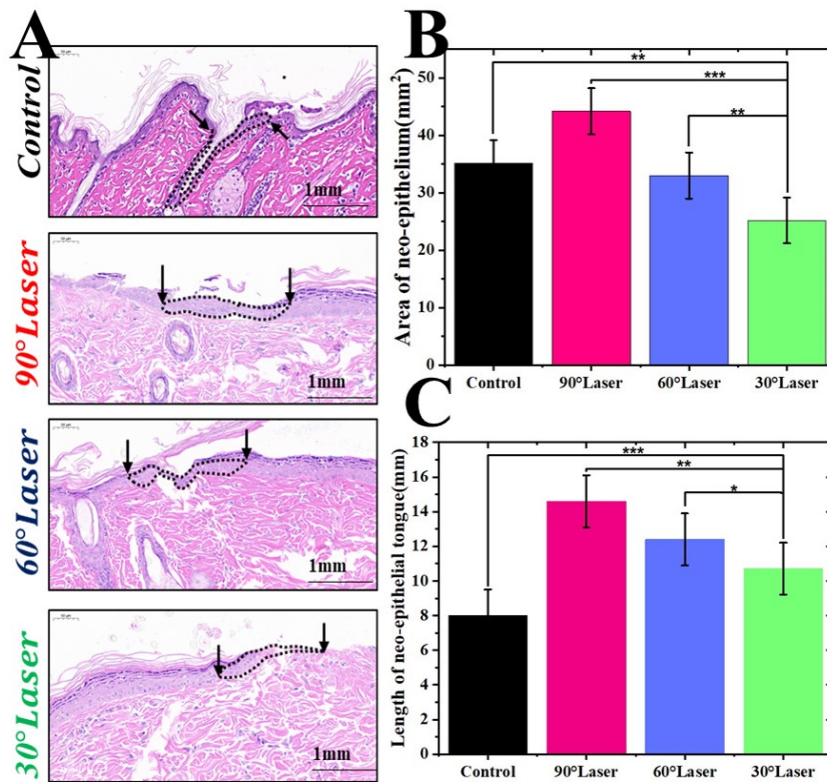


Fig.11 Representative images of thickness of upper epidermis around wound tissue sections in different treatment groups stained by H&E on day 7 (Scale bar $\frac{1}{4}$ 200 μ m). (A) Representative images of wound tissue sections stained by H&E in different treatment groups on day 14 (Scale bar $\frac{1}{4}$ 200 μ m and 10 μ m). (B) Quantification of the epidermis thickness in different treatment groups on day 14 (n $\frac{1}{4}$ 3). Data represent mean \pm SD; *, P \leq 0.05, **, P \leq 0.01, ***, P \leq 0.001.

However, the performance of epithelial regeneration cannot directly correspond to the overall length of healing cycle, it can only reflect the situation of re-epithelialization in the process of wound healing. In general, there are crosses and intersections in all 4 stages of healing. Therefore, in the next section, this paper discussed the indexes including collagen deposition, collagen types and content during the healing process combined with microscopic structures stained by Masson in detail.

Collagen distribution during wound healing

In order to analyze the healing behavior of collagen on the 3rd day after the first laser treatment in detail, it can be seen from the enlarged figure in Fig.12(A) that there were obvious collagen fractures in all groups on the third day, among which the control group had the most significant collagen deposition, the 90deg laser group had the most significant collagen deposition, and the 30deg laser group had the denser morphology of healing. The red fracture is not obvious, while the 60deg laser group has a uniform distribution of fractures [48]. We calculated the collagen content and deposition in the wound area, as shown in Fig.12(B) and (C). The collagen content in the laser affected area of the 90deg laser group was as high as 42.6%, and there was also significant deposition area, which reached 36% of the laser affected area, second only to the 60deg laser group. Although the collagen content of the 30deg laser group reached 34.5%, the deposition area only accounted for 26.3%, indicating that under the laser with large incident angle, there was a tendency to form a dense collagen network structure at this time point, which also explained that the laser affected area of this group of samples was abnormally fine 14 days after healing in Figure 9. In the samples of laser group, the proportion of collagen fractional area was the largest in 60deg laser group, which exceeded 40%. However, according to the above analysis, from the collagen distribution behavior in 14th day of healing (as shown in Fig.13(C)), the collagen network of samples of this group was dense, which was not an optimal healing performance. While the collagen fractional area of 60deg laser group only occupies 34.8%, at 14th day, however, the collagen network structure and fibroblast level of samples in this group were most similar to normal tissues, indicating that the follow-up outstanding healing state could be anticipated by the range of the collagen fractional area, the range could be between 26.3%~40%.

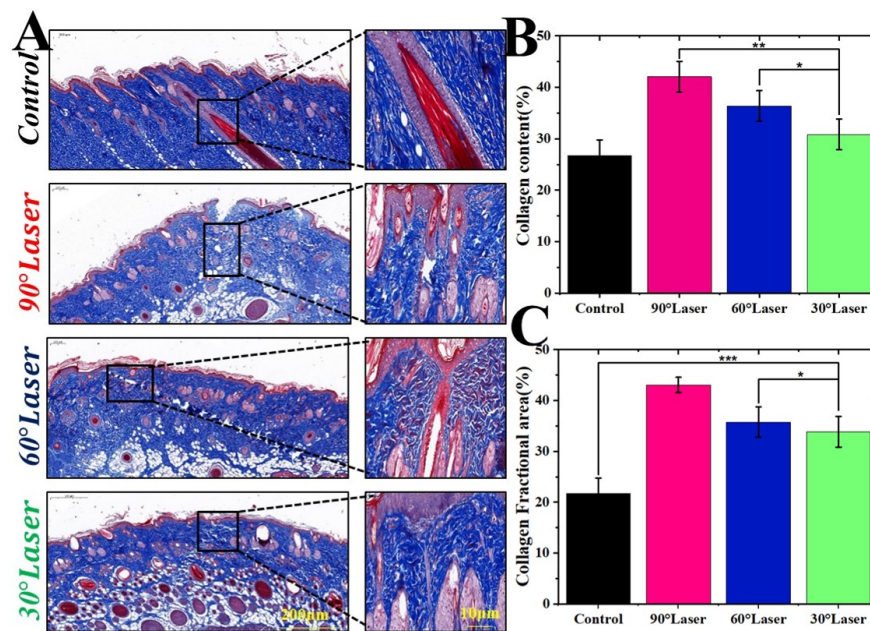


Fig.12(A) Representative images of wound tissue sections stained by Masson in different treatment groups on day 3 (Scale bar $\frac{1}{4}$ 1 mm and 50 μ m). (B) Quantification of the collagen content around laser effect zone in different treatment groups on day 3 ($n = \frac{1}{4} \times 3$). (C) Quantification of the collagen fractional area around laser effect zone in different treatment groups on day 3 ($n = \frac{1}{4} \times 3$).

As shown in Fig.13(A), the wound direction of the four groups of samples on the 3rd day of healing and the distribution of different types of collagens around the wound were separately labeled. It can be observed that the proportion of two types of collagens in the 90° laser group was the most prominent, up to 2.68, and the COL-1 fiber content was significantly higher than that in the other three groups (as shown in Fig.13(C)).

This indicated that the tissue of the samples in this group was relatively stiff after the first laser welding, but the strength was higher, which met the standard of good healing. According to Fig.13(B), the ratio of COL-1 fibers and COL-3 fibers of samples under 90 turned was also the highest. However, the ratio of COL-1 and COL-3 fibers in the samples in two laser groups with incident angles were significantly lower than that in the control group, indicating that although the collagen proliferation of the samples in these two groups was higher than that in the control group without any operation, while COL-3 fiber was the collagen that prolifically proliferated in 60 laser and 30 laser groups, the tissue was softer, and the elasticity was significantly higher than that of the 90° laser group at the 3rd day. After the first laser welding, the higher elasticity of wound tissue indicated that the samples were not prone to scar, and the thermal damage caused by laser was also relatively low under 60 laser and 30 laser.

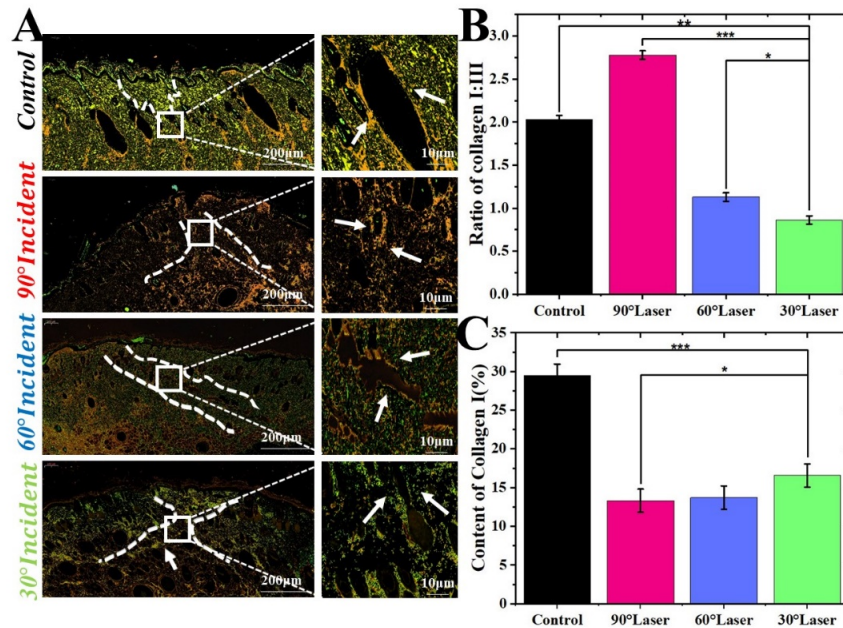


Fig.13 (A) Representative images of wound tissue sections stained by Picrosirius Red in different treatment groups on day 3 (Scale bar $\frac{1}{4}$ 200µm and 10µm). (B) Quantification of the Ratio of collagen I:III in different treatment groups on day 3 (n $\frac{1}{4}$ 3). (C) Quantification of the content of collagen I in different treatment groups on day 3 (n $\frac{1}{4}$ 3)

Next, we need to compare collagen distribution behavior and prognosis in samples after the second laser welding on the 7th day and the 14th day. As shown in Fig.14(A), the deposition area of collagen basically coincides with the proliferation area of COL-1 fiber, indicating that after the second laser welding, the proliferation of COL-1 fiber was mainly stimulated. However, for 90° laser group, the outcome was the opposite. After the second laser welding, the content of COL-1 fiber in the 90° laser group was greatly reduced. On the other hand, the COL-3 fiber content was significantly higher than that after the first stage of laser welding, resulting in ratio of collagen type was only 1.62 on the 7th day. This trend was maintained until the 14th day, when the COL-3 fiber type continued to increase and the ratio of collagen type was only 0.86, lower than normal skin. For the samples of 60° laser group, after the second laser welding, the COL-1 fibers of the samples acquired a large proliferation, and the ratio of collagen type reached 5.2 on the 7th day, which was much higher than other groups for all time points, indicating that the strength of samples could be greatly increased after the second laser welding with 60° incident angle, which laid a good foundation for the subsequent healing process. This also explained the reasons for samples of 60° laser group on the 14th day were the most similar to the collagen structure of normal skin tissue, consistent with the analysis results

after Masson staining, and also explains the rationality of the argument. The collagen type ratio of 30° laser group on the 7th and the 14th day was between 2-2.5, which on the one hand ensured the healing speed and softness of tissue to a certain extent, but also indicated that the proliferation process of COL-1 fibers was much slower. Although the wounds of the samples were completely closed on day 14, the proliferation of COL-1 fibers in the later stage would take longer time^[50].

At the same time, as shown in Fig.14(C), we also calculated the proportion of collagen fiber deposition in samples at these two time points. We found that although the proportion of collagen deposition in the 90° laser group was the highest on the third day, it did not increase significantly after the second laser treatment due to additional thermal damage caused by vertically incident laser. The proportion of collagen deposition in the 60° laser group reached a maximum of 34.6% on day 7, and then continued to increase during the following healing process.

In this section, the distribution of collagen deposition, the proliferation tendency of collagen types and the structure and morphology of collagen network were discussed in detail. In Fig.14(A), it can be seen that the COL-1 fiber distribution of the samples in the 90° laser group is the most significant, and the COL-3 fiber distribution is also very fine. At the same time, the deposition area of collagen network according to Masson staining is also wide and the overall collagen network turned out to be very fine and dense, indicating that the healing process of samples was the fastest under 90° laser welding, but COL-1 collagen was proliferated too much and could be tended to cause scars. The collagen network of the 30° samples also showed fine morphology after Masson staining, but differed from the 90° laser group, the samples of the 30° laser welding showed more COL-3 fibers, and the ratio of two types of collagens were the lowest among all groups, indicating that the skin elasticity was better, but the healing process would be very slow, and there was a tendency of inflammation recurrence in the later stage. On the 14th day, the two staining results of samples under were the closest to normal skin. From the perspective of collagen growth behavior, it can be concluded that 60° laser welding was the most conducive to wound healing.

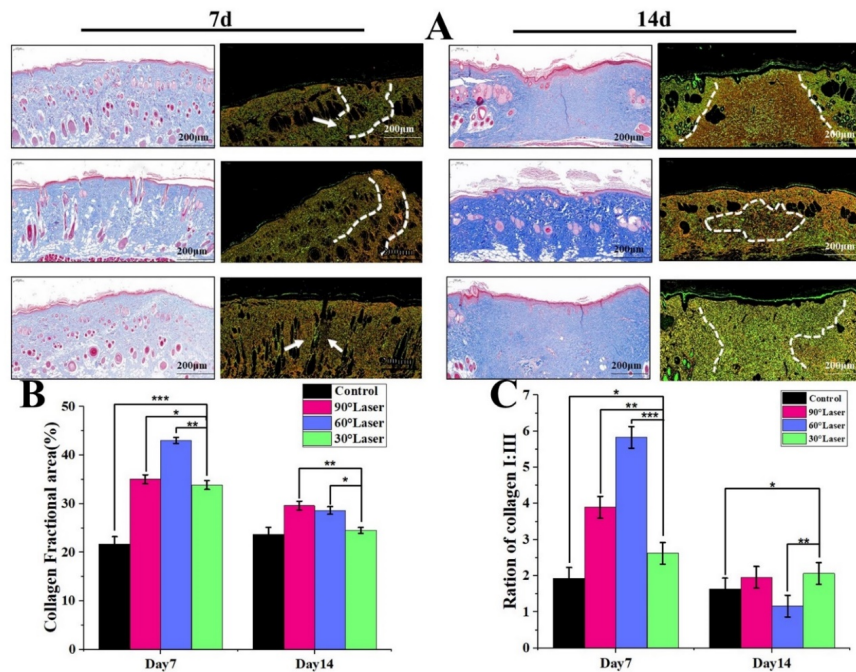


Fig.14 Masson and Picosirius red staining for determination of collagen synthesis in rat model on the 7th and the 14th day. (A) Typical photographs of MTS and Picosirius red staining at Day 7 and 14 of all the groups.

(Scale bar:200 μm). (B) The quantitative results of MTS on collagen deposition. (C) The quantitative results of Picrosirius red staining on the ratio of COL I/III. Data are expressed as the mean \pm SEM; n $\frac{1}{4}$ 3; *P < 0.05; **P < 0.01; ***P < 0.001; ****P < 0.0001.

Conclusion

1. In conclusion, given that a wound occurs at the same position, varying incident angles can significantly influence collagen remodeling behavior around the wound under uniform laser energy conditions. A low-energy 1064nm fiber laser, operating at an energy density of 67.543J/mm², can effectively expedite wound healing in rats. Among various angles tested, a 60° incident angle proved to be the most effective, achieving the fastest healing rate while ensuring optimal collagen network densification and minimized scarring.
2. In vivo observations revealed that low-energy continuous lasers with an incident angle around 60° exhibited superior performance in accelerating wound healing and limiting thermal damage. Furthermore, histological and immunohistochemical analyses corroborated that a 60° laser with an energy density of 67.543 J/cm² could enhance wound cell proliferation, mitigate inflammation, stimulate angiogenesis, and facilitate optimal re-epithelialization.
3. Consequently, low-energy continuous lasers with incident angles around 60° show considerable promise for promoting wound healing in clinical settings. However, it is important to note that the clinical healing of chronic wounds can often be significantly influenced by a patient's underlying health conditions. As such, our laboratory will continue conducting comprehensive research into the effects of low-energy lasers on wound healing in diabetic rats, with the ultimate goal of transitioning this technology into clinical trials in the near future.

Statements & Declarations

Funding

This work was supported by [Qinlan Project of Jiangsu Provienc] (Grant numbers [AD41069]).

Competing Interests

The authors have no relevant financial or non-financial interests to disclose.

Data availability statement

The data that support the findings of this study are available on request from the corresponding author. The data are not publicly available due to privacy or ethical restrictions.

Acknowledgements

All authors contributed to the study conception and design. Material preparation, data collection and analysis were performed by [Yuxin Chen], [Jun Huang], [Kehong Wang]. Animals' experiments were performed by [WenTao Fan]. The first draft of the manuscript was written by [Yuxin Chen] and all authors commented on previous versions of the manuscript. All authors read and approved the final manuscript.

Code, Data, and Materials Availability

No, the manuscript does not have associated code. No datasets were generated or analyzed during the present study. No materials were used for the analysis.

Reference

1. Montagna W. The structure and function of skin[M]. Elsevier, 2012.
2. Liu T, Qiu C, Lu H, et al. A novel recombinant human collagen hydrogel as minced split-thickness skin graft overlay to promote full-thickness skin defect reconstruction[J]. Burns, 2023, 49(1): 169-181.
3. Current therapeutic interventions remain far from ideal repair.
4. Khalkhal E, Razzaghi M, Rostami-Nejad M, et al. Evaluation of laser effects on the human body after laser therapy[J]. Journal of Lasers in Medical Sciences, 2020, 11(1): 91.

5. Wang Z, Zhang B, Liu J, et al. Recent developments in mid-infrared fiber lasers: Status and challenges[J]. *Optics & Laser Technology*, 2020, 132: 106497.
6. Musstaf R A, Jenkins D F L, Jha A N. Assessing the impact of low level laser therapy (LLLT) on biological systems: a review[J]. *International journal of radiation biology*, 2019, 95(2): 120-143.
7. Khalkhal E, Rezaei-Tavirani M, Zali M R, et al. The evaluation of laser application in surgery: a review article[J]. *Journal of lasers in medical sciences*, 2019, 10(Suppl 1): S104.
8. Ahluwalia J, Avram M M, Ortiz A E. Lasers and energy-based devices marketed for vaginal rejuvenation: A cross-sectional analysis of the MAUDE database[J]. *Lasers in surgery and medicine*, 2019, 51(8): 671-677.
9. Salem U, Kumar V A, Madewell J E, et al. Neurosurgical applications of MRI guided laser interstitial thermal therapy (LITT)[J]. *Cancer Imaging*, 2019, 19(1): 1-13.
10. Bianchi L, Cavarzan F, Ciampitti L, et al. Thermophysical and mechanical properties of biological tissues as a function of temperature: A systematic literature review[J]. *International Journal of Hyperthermia*, 2022, 39(1): 297-340.
11. Mohammadi A, Bianchi L, Asadi S, et al. Measurement of ex vivo liver, brain and pancreas thermal properties as function of temperature[J]. *Sensors*, 2021, 21(12): 4236.
12. Sur A, Mondal S, Kanoria M. Influence of moving heat source on skin tissue in the context of two-temperature memory-dependent heat transport law[J]. *Journal of Thermal Stresses*, 2020, 43(1): 55-71.
13. Sur A, Mondal S, Kanoria M. Influence of moving heat source on skin tissue in the context of two-temperature Caputo–Fabrizio heat transport law[J]. *Journal of Multiscale Modelling*, 2020, 11(02): 2050002.
14. Prawatborisut M, Jiang S, Oberlander J, et al. Modulating Protein Corona and Materials–Cell Interactions with Temperature-Responsive Materials[J]. *Advanced Functional Materials*, 2022, 32(2): 2106353.
15. Zuev V M, Kalinina E A, Kukushkin V I, et al. Innovative laser technologies in the diagnosis and treatment of the endometrium of concern in reproductive medicine[J]. *Obstetrics and Gynecology*, 2020 (4): 157-165.
16. Digesu G A, Tailor V, Preti M, et al. The energy based devices for vaginal “rejuvenation,” urinary incontinence, vaginal cosmetic procedures, and other vulvo-vaginal disorders: An international multidisciplinary expert panel opinion[J]. *Neurourology and urodynamics*, 2019, 38(3): 1005-1008.
17. Hu T, Lo A C Y. Collagen–Alginate Composite Hydrogel: Application in Tissue Engineering and Biomedical Sciences[J]. *Polymers*, 2021, 13(11): 1852.
18. Yang X, Deng H, Lv J, et al. Comparison of changes in adipokine and inflammatory cytokine levels in patients with newly diagnosed type 2 diabetes treated with exenatide, insulin, or pioglitazone: a post-hoc study of the CONFIDENCE trial[J]. 2023.
19. Zhou R, Bu W, Fan Y, et al. Dynamic Changes in Serum Cytokine Profile in Rats with Severe Acute Pancreatitis[J]. *Medicina*, 2023, 59(2): 321.
20. Alanazi R S, Laref A. Monte Carlo Simulations of the photo-thermal cancer therapy of melanin[J]. *Indian Journal of Physics*, 2021, 95(12): 2589-2605.
21. Zhang B, He J, Shi M, et al. Injectable self-healing supramolecular hydrogels with conductivity and photo-thermal antibacterial activity to enhance complete skin regeneration[J]. *Chemical Engineering Journal*, 2020, 400: 125994.
22. Chen C, Xi Y, Weng Y. Progress in the Development of Graphene-Based Biomaterials for Tissue Engineering and Regeneration[J]. *Materials*, 2022, 15(6): 2164.
23. Hobiny A, Alzahrani F, Abbas I, et al. The effect of fractional time derivative of bioheat model in skin tissue induced to laser irradiation[J]. *Symmetry*, 2020, 12(4): 602.
24. Luke A M, Mathew S, Altawash M M, et al. Lasers: A review with their applications in oral medicine[J]. *Journal of lasers in medical sciences*, 2019, 10(4): 324.
25. Yu L, Hao L, Meiqiong T, et al. The medical application of terahertz technology in non-invasive detection of cells and tissues: opportunities and challenges[J]. *RSC advances*, 2019, 9(17): 9354-9363.
26. Huang J, Chen Y, Chen Z, et al. Effects of scanning paths on laser welding[J]. *Optics and Lasers in*

- Engineering, 2020(130),106078.
27. Li C, Huang J, Wang K, et al. Optimization of processing parameters of laser skin welding in vitro combining the response surface methodology with NSGA-II[J]. *Infrared Physics & Technology*, 2019, 103: 103067.
 28. Li C, Huang J, Wang K, et al. Investigation on thermal damage model of skin tissue in vitro by infrared laser welding[J]. *Optics and Lasers in Engineering*, 2020, 124: 105807.
 29. Wick M R. The hematoxylin and eosin stain in anatomic pathology—An often-neglected focus of quality assurance in the laboratory[C]//*Seminars in diagnostic pathology*. WB Saunders, 2019, 36(5): 303-311.
 30. Foot N C. The Masson trichrome staining methods in routine laboratory use[J]. *Stain technology*, 1933, 8(3): 101-110.
 31. Rich L, Whittaker P. Collagen and picrosirius red staining: a polarized light assessment of fibrillar hue and spatial distribution[J]. *Journal of morphological sciences*, 2017, 22(2): 0-0.
 32. Mendes J J, Leandro C I, Bonaparte D P, et al. A rat model of diabetic wound infection for the evaluation of topical antimicrobial therapies[J]. *Comparative medicine*, 2012, 62(1): 37-48.
 33. Butler J E. Enzyme-linked immunosorbent assay[J]. *Journal of immunoassay*, 2000, 21(2-3): 165-209.
 34. Hakkinen L, Larjava H, Koivisto L. Granulation tissue formation and remodeling[J]. *Endodontic Topics*, 2011, 24(1): 94-129.
 35. Utsunomiya H, Tilakaratne W M, Oshiro K, et al. Extracellular matrix remodeling in oral submucous fibrosis: its stage-specific modes revealed by immunohistochemistry and in situ hybridization[J]. *Journal of oral pathology & medicine*, 2005, 34(8): 498-507.
 36. Bertolotti E, Malagoli D, Franchini A. Skin wound healing in different aged *Xenopus laevis*[J]. *Journal of morphology*, 2013, 274(8): 956-964.
 37. Lucas T, Waisman A, Ranjan R, et al. Differential roles of macrophages in diverse phases of skin repair[J]. *The Journal of Immunology*, 2010, 184(7): 3964-3977.
 38. Enoch S, Leaper D J. Basic science of wound healing[J]. *Surgery (Oxford)*, 2008, 26(2): 31-37.
 39. Amadeu T P, Seabra A B, de Oliveira M G, et al. Nitric oxide donor improves healing if applied on inflammatory and proliferative phase[J]. *Journal of Surgical Research*, 2008, 149(1): 84-93.
 40. Tang J, Liu H, Gao C, et al. A small peptide with potential ability to promote wound healing[J]. *PloS one*, 2014, 9(3)
 41. Hong Y K, Lee Y C, Cheng T L, et al. Tumor endothelial marker 1 (TEM1/Endosialin/CD248) enhances wound healing by interacting with platelet-derived growth factor receptors[J]. *Journal of Investigative Dermatology*, 2019, 139(10): 2204-2214.
 42. Yang Y, Yu C, Le Y, et al. Angiopoietin-like 4 promotes the proliferation and migration of epidermal stem cells and contributes to the re-epithelialization of cutaneous wounds[J]. *bioRxiv*, 2023,729672.
 43. Solan A, Mitchell S, Moses M, et al. Effect of pulse rate on collagen deposition in the tissue-engineered blood vessel[J]. *Tissue engineering*, 2003, 9(4): 579-586.
 44. Gemmiti C V, Guldberg R E. Fluid flow increases type II collagen deposition and tensile mechanical properties in bioreactor-grown tissue-engineered cartilage[J]. *Tissue engineering*, 2006, 12(3): 469-479.
 45. Hallock G G, Merkel J R, Rice D C, et al. The ontogenetic transition of collagen deposition in rat skin[J]. *Annals of plastic surgery*, 1993, 30(3): 239-243.
 46. Savani R C, Hou G, Liu P, et al. A role for hyaluronan in macrophage accumulation and collagen deposition after bleomycin-induced lung injury[J]. *American journal of respiratory cell and molecular biology*, 2000, 23(4): 475-484.
 47. Lu Q L, Zheng Z X, Ye Y H, et al. Macrophage migration inhibitory factor takes part in the lumbar ligamentum flavum hypertrophy[J]. *Molecular Medicine Reports*, 2022, 26(3): 1-9.
 48. Xu Y, Deng M, Cai Y, et al. Cell-free fat extract increases dermal thickness by enhancing angiogenesis and extracellular matrix production in nude mice[J]. *Aesthetic surgery journal*, 2020, 40(8): 904-913.
 49. Liu X, Wu H, Byrne M, et al. Type III collagen is crucial for collagen I fibrillogenesis and for normal cardiovascular development[J]. *Proceedings of the National Academy of Sciences*, 1997, 94(5): 1852-1856.

50. Fleischmajer R, Perlish J S, Burgeson R E, et al. Type I and type III collagen interactions during fibrillogenesis[J]. *Annals of the New York Academy of Sciences*, 1990, 580: 161-175.
51. Structure and function of collagen types[M]. Elsevier, 2012.
52. Bornstein P, Sage H. Structurally distinct collagen types[J]. *Annual review of biochemistry*, 1980, 49(1): 957-1003.
53. Bohm S, Strauss C, Stoiber S, et al. Impact of source and manufacturing of collagen matrices on fibroblast cell growth and platelet aggregation[J]. *Materials*, 2017, 10(9): 1086.
54. Xu Z, Chen D, Hu Y, et al. Anatomically distinct fibroblast subsets determine skin autoimmune patterns[J]. *Nature*, 2022, 601(7891): 118-124.
55. Mascharak S, Longaker M T. Fibroblast heterogeneity in wound healing: hurdles to clinical translation[J]. *Trends in molecular medicine*, 2020, 26(12): 1101-1106.
56. Oh E J, Gangadaran P, Rajendran R L, et al. Extracellular vesicles derived from fibroblasts promote wound healing by optimizing fibroblast and endothelial cellular functions[J]. *Stem Cells*, 2021, 39(3): 266-279.
57. Abbasi S, Sinha S, Labit E, et al. Distinct regulatory programs control the latent regenerative potential of dermal fibroblasts during wound healing[J]. *Cell stem cell*, 2020, 27(3): 396-412.
58. Shabestani Monfared G, Ertl P, Rothbauer M. An on-chip wound healing assay fabricated by xurography for evaluation of dermal fibroblast cell migration and wound closure[J]. *Scientific reports*, 2020, 10(1): 16192.